

ARTICLE

Highly Transferable Atomistic Machine-Learning Potentials from Curated and Compact Datasets Across the Periodic Table

Received 00th January 20xx,
Accepted 00th January 20xx

DOI: 10.1039/x0xx00000x

Christopher M. Andolina^a and Wissam A. Saidi^{*,a,b}

Machine learning atomistic potentials (MLPs) trained using density functional theory (DFT) datasets allow for the modeling of complex material properties with near-DFT accuracy while imposing a fraction of its computational cost. The curation of the DFT datasets can be extensive in size and time-consuming to train and refine. Herein we focus on addressing these barriers by developing minimalistic and flexible datasets for many elements on the periodic table regardless of mass, electron configuration, and ground state lattice. These DFT datasets have, on average, ~4000 different structures and 27 atoms per structure, which we found sufficient to maintain predictive accuracy of DFT properties and notably with high transferability. We envision these highly curated training sets as starting points for the community to expand, modify, or use with other machine learning atomistic potential models, whatever may suit individual needs, further accelerating the utilization of machine learning as a tool for materials design and discovery.

1. Introduction

A large body of work describing code development, training, validation, and transferability of machine learning atomistic potentials (MLPs) has recently been reported, highlighting notable and significant advances in materials modeling.¹⁻⁴ Many of these studies underscore that MLPs have high fidelity in simulating different properties and are significantly less computationally demanding than density functional theory (DFT) calculations.⁴ Therefore, MLPs can readily be used to model known materials at large sizes (a recent study claiming ten billion atoms⁵) and long timescales and to discover applications of interest⁶, all while further accelerating the computational modeling of materials⁷. Recent refinements of machine learning (ML) approaches^{8, 9} and training methodologies^{7, 10} have further improved the accuracy, precision, and utility of these atomistic potentials and their use for various material applications.¹¹ Computational material science has seized upon the development of these ML advances for chemical modeling applications¹² and applied them to describe complex dynamics systems ranging from single elementals¹³, bimetallic systems¹⁴⁻¹⁶, supported metal nanoclusters¹⁷, hybrid perovskites¹⁸, and metal oxides¹⁹. Although MLPs, in general, are less time-consuming to train/refine and more robust at describing systems outside of

their training datasets (transferability)²⁰⁻²³ compared to classical atomistic potentials (e.g., embedded atom model potentials), the training workflow and database composition are areas that could benefit from further optimization as noted in current reviews of the literature^{24, 25}.

We aim to further advance MLP development by providing a clear and systematic approach to curating minimalistic DFT datasets that can be applied to almost any element on the periodic table (Figure 1). Creating databases to train ML potentials is a challenging endeavor, on its own, regardless of the ultimate application of the atomistic potential²⁶. Herein, we focus on using deep neural network models to develop atomistic potentials. Although we specifically examine the predictive accuracy of the deep neural network potentials (DNP) with these DFT datasets, we expect other MLP models to have a similar accuracy based on prior investigations²⁷. We note there are few examples of these highly applicable methodologies for multiple (over 23) elements²⁸ distinct from this approach and rely on the automated workflows of DP-GEN²⁹.

We demonstrate our approach by sampling elements with distinct masses, electron configurations, and ground-state crystal phases (excluding the rare earth elements). Our method for developing single-element datasets relies on the curated Material Project database (MPDB)³⁰ and the NOMAD repository and archive³¹, and a DeePMD-kit neural network approach³². We refine our DNP models using adaptive learning. We apply an ensemble approach to compare single-element inter-DNP deviations of randomly seeded models and select configurations with the more significant force deviations for further training. The final single-element potentials were trained up to three iterations, containing less than 3857 ± 1032 with an overall average of 27 ± 12 atoms per structure (see Table S1 for more details). These DNPs can accurately predict

^a Department of Mechanical Engineering and Materials Science, University of Pittsburgh, Pittsburgh, PA 15261 USA

^b National Energy Technology Laboratory, United States Department of Energy, Pittsburgh, PA 15236 USA.

Electronic Supplementary Information (ESI) available: [details for all DNP and DFT values for each lattice, point defect, elastic constant, and surface that was presented in the plots. As well as configuration counts for the training data.]. See DOI: 10.1039/x0xx00000x. DFT training data, DNPs, and example validation scripts can be found here (<https://github.com/saidigroup/23-Single-Element-DNPs>).

several properties of five low-energy lattice configurations for each element. As shown below, the resulting potentials have good transferability to atomic environments not explicitly included in the training database (e.g., other lattice configurations, vacancies, surfaces, and thermal stability of the solid phase).

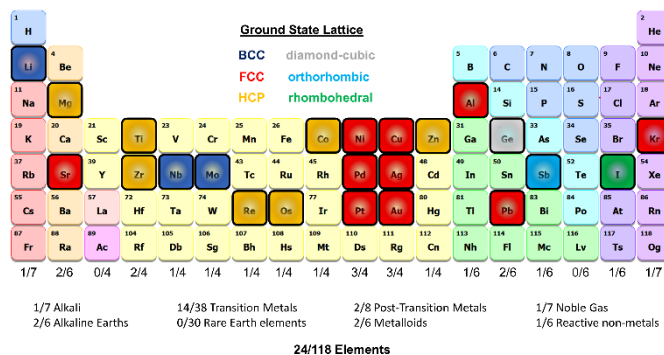


Figure 1. Schematic of the Period Table visualizing the elements selected for this work and highlighting ground state lattice configurations.

2. Computational Methods

2.1 Curation of the DFT Dataset for DNP Training.

Initial DFT parent structures consisted of five of the lowest energy lattice structures deposited in MPDB³³ (e.g., face-center-cubic (fcc), body-center-cubic (bcc), hexagonal, hexagonal close-pack (hcp), rhombohedral, orthorhombic, tetragonal, trigonal, simple cubic, and/or diamond cubic.) If five structures were not located in the MPDB for a select element, additional lattice crystal systems were obtained from the NOMAD Repository and Archive³¹ or generated³⁴ and optimized using DFT (VASP)³⁵⁻³⁷ before training. The specific lattices used for training vary from element to element; the electronic supporting information (ESI) notes a complete list of phases (**Table S2**). Generally, for the ground state configuration, single-point defect structures (vacancy **Table S4** or interstitial **Table S5**) were generated from a DFT-optimized 2x2x2 supercell of the conventional lattice structure. Additionally, each dataset contained a set of deformed lattices in twelve directions, typically employed to calculate elastic constants from finite differences. For each parent structure (point defect type and each of the 12 deformed lattices), 20 configurations were generated from a molecular dynamics (MD) trajectory with constant volume and temperature (NVT) at two temperatures (T_m and 0.25 T_m) for the elements with melting temperatures T_m at < 2000 K, and three temperatures (T_m , 0.6 T_m and 0.25 T_m) for select elements with $T_m > 2000$ K.

The VASP calculations were performed using Perdew-Burke-Ehrenzhof (PBE) exchange-correlation functional with projector-augmented wave pseudopotentials³⁵⁻³⁷, which correspond to those used by the corresponding elements listed in the MPDB^{33, 38}. We selected a plane-wave cut-off of 400 eV that was used consistently across all materials. We used a tight break condition of 10^{-8} eV free energy change between steps in

the electronic relaxation loop. Moreover, we applied Methfessel-Paxton³⁹ smearing of 2nd-order with 0.15 eV, broadening to sample the Brillouin zone. We used a k-spacing value of 0.24 Å⁻¹ for all calculations, which we previously showed to be sufficient for training purposes as DNPs generated using the DFT training database were found to be less sensitive to errors from under-sampling the Brillouin zone than the standard DFT calculations¹³.

2.2 Description of DNP Training Procedure

Machine learning potentials were trained using DeePMD-kit (v2.1.2)⁴⁰ within the DeepPot-SE⁴¹ approach. DeePMD-kit utilizes neural networks to interpolate the relationship between atomic coordinates (model input samples) and the energies, forces, and virials (model output labels) in DFT training data. We used a consistent training protocol with identical hyperparameters for each DNP, including randomly initialized weights in the neural networks. The complete set of hyperparameters used for training is provided in a DeePMD-kit input file in the ESI.

Three DNPs with initial randomized weights were generated at each step of the iterative training process. LAMMPS was utilized to calculate various properties (*vide infra*) for each element. The averages and standard deviations of the DNPs-calculated properties were examined and compared to VASP reference properties with the same initial structures to determine the overall accuracy and precision of the potential. At least two training iterations (iterations 0 and 1) were performed for every element to hone the DNP accuracy.

2.2.1 Adaptive Learning

All subsequent training iterations beyond the initial dataset (iteration 0) were generated by an "adaptive-learning" (iterations 1, 2, or 3) process utilizing the same initial structures used to create the iteration 0 dataset. We used force-based criteria to select additional configurations (0.07 to 2 eV/Å) to be included in the next iteration of the DNP training utilizing LAMMPS NVT ensemble approach with the DeePMD-kit, outside of the force tolerance range. We then generated up to ten new DFT structures using VASP NVT to train each structure. Again, as with the validation of "iteration 0", the mean of the material properties (and the standard deviation of the mean) were compared to the VASP reference values to verify improved DNP accuracy. The process was repeated until the computed cohesive energies (E_{coh}) and per atom volumes were $\leq 12\%$ of the corresponding DFT reference values (**Figure 2, Table S2**).

2.2 DFT Reference Values

DFT material property references were calculated for the five lattices used as training data sets using VASP parameters similar to the training dataset. For basic lattice properties such as lattice constants, unit cell volume per atom, and cohesive energy (E_{coh}), we used a conventional primitive unit cell (1x1x1) and previously reported methodologies¹⁶. For single atom vacancies and interstitials, we used a 2x2x2 supercell.

Elastic constant calculations were made using VASP with the same convergence thresholds, 2x2x2 supercell (if the conventional cell contained \leq four atoms), IBRION value of six, and NFREE value of two. All other parameters were the same for the VASP static property calculations, including the energy cut-off of 400 eV. We used a POTMIN value of 0.01 Å, for the atomic displacements. Our values generally agree with the elastic constant reported in the MPDB⁴² (Table S5).

2.4 LAMMPS Calculations

We have detailed descriptions of our process to calculate material properties using LAMMPS and the DNP reported elsewhere in the literature¹³⁻¹⁶. We used convergence criteria based on 1×10^{-10} eV for energy and forces between minimization steps. A 4x4x4 supercell was used for elastic calculations with a 0.005-0.01 Å displacement.

Continuous heating curves for validation are obtained from molecular dynamics simulations employed within a NVT ensemble with one femtosecond timestep. The temperature was controlled using a Berendsen thermostat applied every 100 steps. The temperature was ramped (1 K / femtosecond) from 0 K to approximately 100 K above the experimental melting temperatures starting with a ground-state lattice supercell relaxed at 0 (bar) pressure. We used 10x10x10 supercells for each element's identified ground-state lattice structure. We utilized a compressed version of the DNP for these MD heating simulations, which improved the speed of the simulation with a negligible impact on the accuracy of this calculation.

2.5 Validation Check on Non-trained Structures.

We assess the transferability of DNP for each element on structures not explicitly included in the training. Some of the structures were gathered from The MPDB some were generated⁴³ by our group. We compared DNP calculated and averaged cohesive energy (E_{coh}), per atom volume, and elastic constants to DFT reference values (Tables S8-10).

2.6 Surface Energy Calculations

We utilized the LAVA code⁴⁴ to calculate low energy non-reconstructed Miller index surfaces (100), (110), and (111) (fcc, bcc, and diamond cubic phases and (0001), (10 $\bar{1}$ 0) and (11 $\bar{2}$ 0) for the hcp phase) surface energies using the LAMMPS wrapper with the DNP. The average surface energies were determined from the three randomly seeded DNP and compared to corresponding DFT (VASP) calculated reference values from the MPDB⁴⁵.

3. Results and Discussion

We developed a simplistic approach for generating and refining the DFT training dataset for 23 elements (Ag, Al, Au, Co, Cu, Ge, I, Li, Kr, Nb, Ni, Mg, Mo, Os, Pb, Pd, Pt, Re, Sb, Sr, Ti, Zn, and Zr) across the periodic table (Figure 1) to develop robust DNP, which describe base material properties for many temperatures, various phases, and selected point defects. The elements chosen in this study represent a wide range of melting

temperatures (e.g., Kr and Os), atomic masses (e.g., Li and Pb), electron configurations, elemental groups, and ground state phases (11 x fcc, 6x hcp, 2x bcc, 1x diamond cubic, 1 x tetragonal, 2 x orthorhombic). Applying these simplified and compact DFT training set criteria to a diverse selection of elements strongly suggests that this general approach applies to most elements on the periodic table for dataset creation, modeling, and refinement for DNP, at least for single-element systems. We did not investigate the impact of tailoring the model's hyperparameters to each element training dataset which may improve accuracy and performance; instead, we chose to use a "universal" set of parameters for all elements. Our dataset curation focused on achieving good accuracy of lattice constants, cohesive energies, single vacancy defects, interstitial atoms, elastic constants, and thermal stability of the solid phase between 0 K and the melting temperature.

To generate the 12 distortions of the lattice in the elastic limit for each lattice of the metal systems, we tested a variety of thresholds from 0.01 to 0.05 Å. We found that distortions of the lattice by 0.03 Å yielded DNP that produced the most accurate results overall with the smallest number of configurations. We ran NVT at the previously defined temperature(s) for each distorted structure to generate 20 configurations. Additionally, we included single vacancy structures for each phase and a variety of self-interstitials (see below) for only the lowest energy phase of each element. We note that, at most, two additional adaptive learning training iterations were required, in addition to the initial training set to produce elastic properties that we considered converged with our calculated DFT reference values. The general workflow is depicted in (Figure 2).

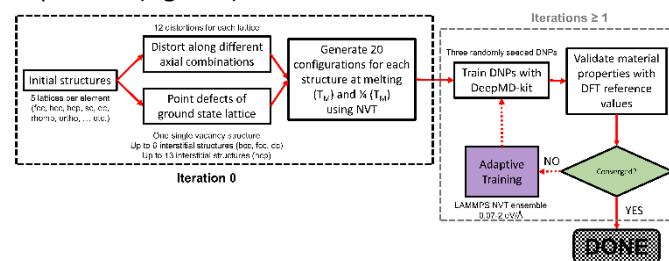


Figure 2. General training workflow for the single-element DNP.

As an additional quality check on the precision of the DNP, while the training improves from iteration to iteration, the standard deviation between the three randomly seeded potentials decreases. We believe this ensemble approach to DNP validation is an important metric to highlight as we envision these DFT datasets as a minimalistic "core" dataset that can be added to or combined for tailored applications by the community. Reporting the average value and the standard deviation of the values from three DNP allows others to assess the precision of the potential and determine whether these values are acceptable for their desired application or if more training will be required. Overall, the maximum number of configurations used for training was less than 6100, with no more than 231,000 total atoms per element (Table S1).

3.1 Basic Material Properties and Phases

We find excellent agreement between the predicted DNP and the DFT reference values for lattice constants and cohesive energies (Figure 3, Tables S2 and S3), exemplified by the proximity to the parity line and relatively small standard deviations shown in Figure 2. The percent deviation from the DFT reference values is < 12 % (excluding Kr, which has very small cohesive energies) per atom volume and < 11 % for cohesive energies (E_{coh}). The errors reported in the figures and the ESI tables are the standard deviation of the averaged material property from the three randomly seeded DNP potentials. Notably, we did not include any of these structures in the training datasets in the training data sets; only distorted or defected lattices at temperatures above 0 K, yet the prediction of the DNPs is accurate compared to DFT reference values reflecting its transferability.

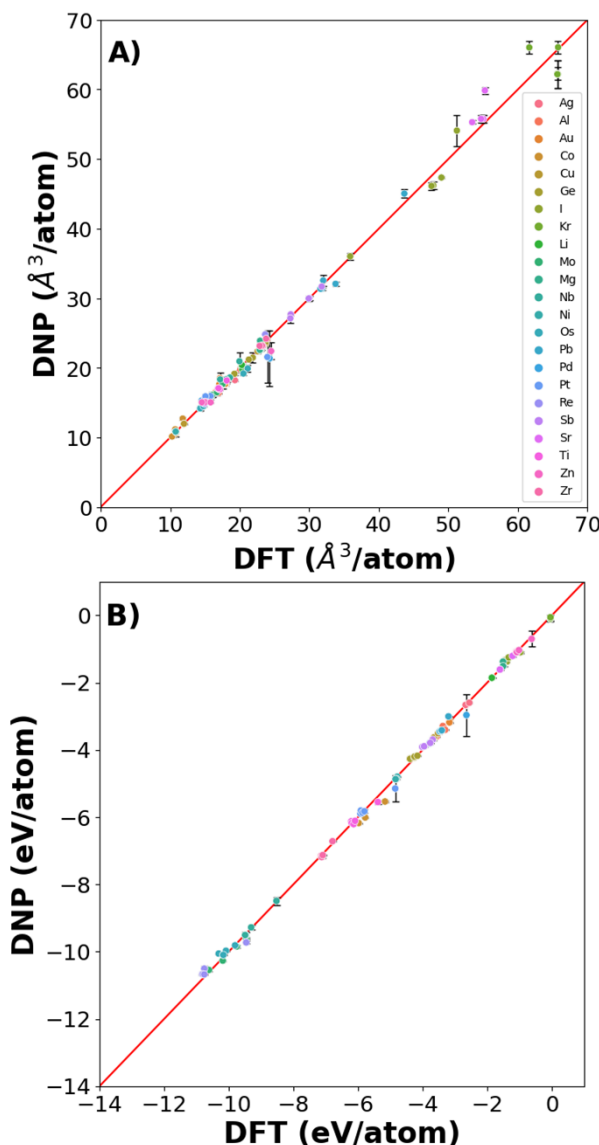


Figure 3. Parity plot of A) cell volume/atom and B) cohesive energies for all elements and phases.

3.2 Point Defects: Vacancies and Interstitials

Real-world materials are not pristine, containing defects such as vacancies and interstitials. Therefore, these common point defects were included in the training data sets for each element to improve the basic DNP applicability to real-world materials modeling (Figures 4 and 6). We compare structures included and excluded in training for single vacancy defect energies (Figure 4A and Table S4). The vacancy energies can be relatively small (less than an eV), so some structures' standard deviations appear more pronounced. Generally, we observe good agreement for most vacancy energies. However, we do not achieve the same accuracy for the energies of the non-defected ground state lattices exemplified in Figure 3.

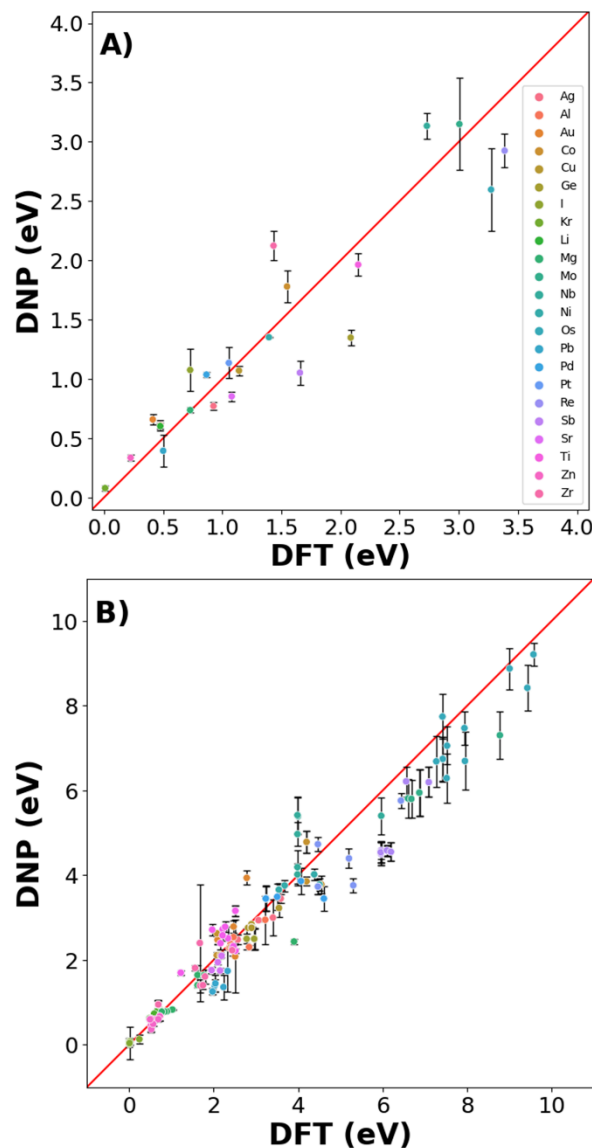


Figure 4. Parity plot of point defects A) vacancies B) single self-interstitial atom energies.

For the self-interstitial facilities, we looked at a large variety of tetrahedral (T_d), octahedral (O_h), dumbbell (db), and crowdion for the lowest energy/ground state phase for each element provided the phase was bcc⁴⁶, fcc⁴⁶, diamond cubic⁴⁷, or hcp⁴⁸ (**Figure 4B** and **Table S5**). We observe good agreement between the average DNP value and the calculated DFT value; however, we note that few interstitials exhibit significant standard deviations of the mean. Upon closer scrutiny, corresponding interstitials were deemed unstable, as the initial and final structures exhibited an unusual change in the cell volume in the DFT reference calculations, therefore, were omitted from validation (**Figure 4** and **Table S5**).

3.3 Elastic Constants

Generating DNPs that accurately predict elastic constants for multiple lattice phases per element is challenging, given that this relies on finite differences. Such has not been frequently reported in the literature^{19, 49}. **Figure 5** compares the DNP and DFT calculation results for unique elastic constants (C_{11} , C_{12} , C_{13} , C_{22} , C_{33} , C_{44} , C_{55} , and C_{66}) for each element's ground state phase (**Table S6**). DFT calculations of elastic constants can be highly sensitive to cut-off energies, kgrid spacings, and supercell size¹³. We observe a more significant standard deviation for the elements with heavier nuclei and unfilled electron shells (e.g., Os and Re). Therefore, the observed standard deviations scale with the magnitude of the average value of the elastic constant.

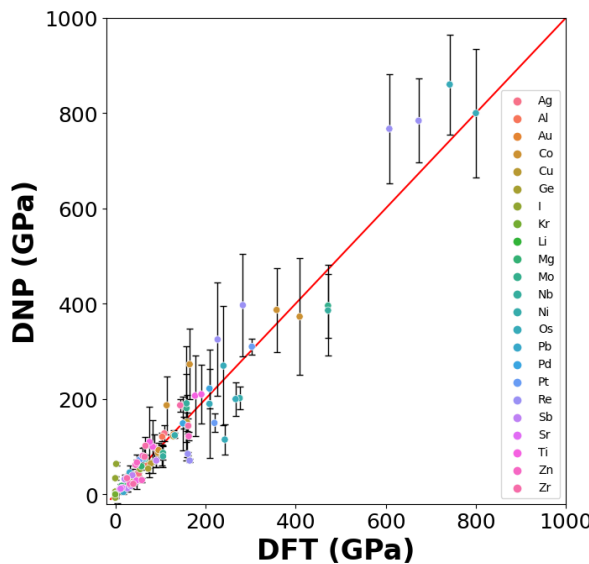


Figure 5. Calculated DNP and DFT elastic constants.

3.4.1 Summary

We summarize our training validation results in **Table S7**, which highlights the % deviations of the DNP from that of the DFT reference values (**Tables S2, S4-6**, and **Figures 3-5**) for each parameter class. Generally, the average error in the per atom volume and E_{coh} are less than 5%, excluding Krypton (**Table S2** and **Table S7**) which has relatively small cohesive energy (~ 0.04-0.08 eV). Similarly, we observe a trend of larger % deviations point defect energies

increases. However, the % E_{coh} for these point defect structures is less than 10% (excluding Kr) from the DFT reference. Minor deviations from the DFT reference value 0.01-0.02 eV in both the pristine and defected can lead to significant errors in the calculated defect energy. Elastic constants are ≤ 25 % in error for most elements on average. However, we observe, on average, larger discrepancies for Pb, Re, Sb, Ti, Zn, and Zr (**Table S7**). These deviations can be further reduced with additional training focused on these structures. Overall the observed variations are similar to what Zuo et al.²⁷ described for multiple MLP models. We note, however, that Zuo et al. trained on a single lattice phase, and the transferability of the MLPs was not thoroughly explored.

3.5.1 Transferability of the DNPs

The transferability of a DNP reflects its ability to accurately predict structures or properties structures that were not included in the training set. Our previous work noted good transferability of the DNP^{14, 15}.

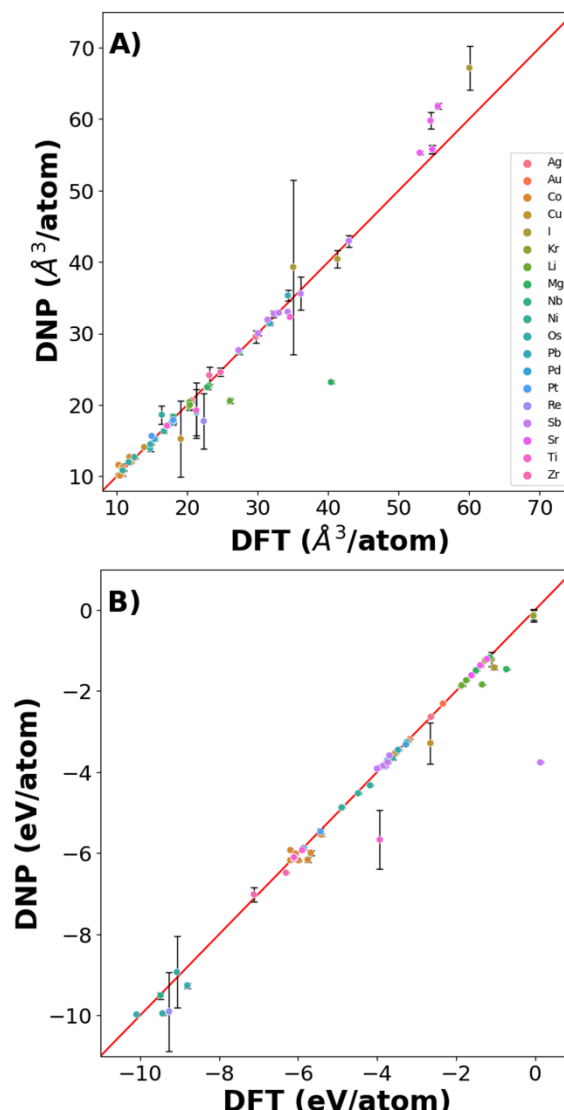


Figure 6. DNP Predictive accuracy for elemental phases not included in the training dataset for A) Volume/atom and B) Cohesive energy.

Here we start examining the transferability by testing a limited number of phases (either from the MPDB or generated by us) per element and comparing them to DFT reference values.

Figure 6 shows that the potentials predict the per atom volume (**Figure 6A**) and E_{coh} (**Figure 6B**) well, with only a small number of structures where E_{coh} and per atom volumes were poorly predicted (**Figure 6** and **Table S9**). However, the % average vacancy energy error (and standard deviation) in the single atom vacancy is more significant than we observed for the trained structures, respectively (**Tables S4** and **S10**), highlighting the boundaries of DNP transferability.

Additionally, comparing elastic constant for non-groundstate phases demonstrates agreement with DFT reference values (**Table S8**). Although the agreement is less than desirable for some of these lattices, additional training would be necessary to describe the untrained vacancies and non-refined elastic constant predictions. However, the overall transferability of these simple phases and point defects is remarkable. Further, these DNPs can be extended to other properties.

3.5.2 Surface Energies

Surface energies are essential properties for materials for understanding material growth, adsorbate behavior, and catalytic performance.^{50, 51} Despite the importance of planar structures, we did not include these in the initial training to reduce the size of the dataset. However, as shown in **Figure 7**, the DNPs predict surface energies reasonably well for low Miller index structures (*e.g.*, fcc, bcc, diamond- (001) (011), and (111); or hcp – (0001), (1010), and (1120)) (**Table S11**). Although further training is required to improve the accuracy of the surface energy predictions, the transferability of these DNPs is surprising as we have not introduced any aperiodic structures resembling a surface in the training set.

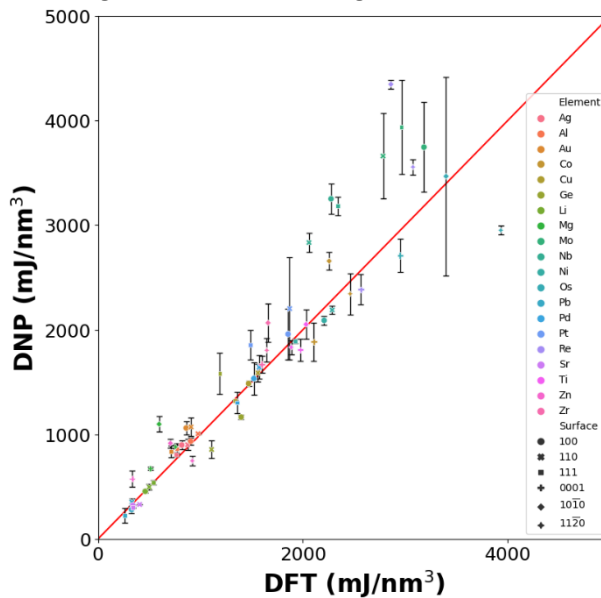


Figure 7. DNP prediction of low Miller index surfaces (< 2) for selected elements compared with DFT reference values. The DNPs are trained only on bulk configurations.

3.5.3 Thermal Stability of the Solid Phase

As a final assessment of these DNPs' robustness, we conducted MD simulations from 0 K approaching each element's melting temperature (**Figure 8**) using an NVT approach and a Berendsen thermostat. During the iterative training, we observed poor thermal stability for the elements with relatively high melting temperatures (above 2000 K). This leads us to include an additional group of training data at a temperature of 60% of the melting point. Including these data vastly improved the solid-state thermal stability up to the melting temperature and improved the initial (iteration 0) predictions of the elastic constants. Even though the training data set only included two temperatures, we found well-behaved heating of these elemental bulk materials with supercells of 10x10x10 for each element's ground state configuration. This result is surprising but not wholly unexpected given that the interpolation of the material properties using DNPs has been noted by us¹⁴⁻¹⁶ and others in the literature⁵². We note that the training did not explicitly include the structures describing liquid phase behavior; therefore, we do not expect the phase transition from solid to liquid to be reasonably predicted for all these elemental DNPs. Future investigations focusing on the refinement of modeling solid-liquid phase transitions are the focus of ongoing investigations.

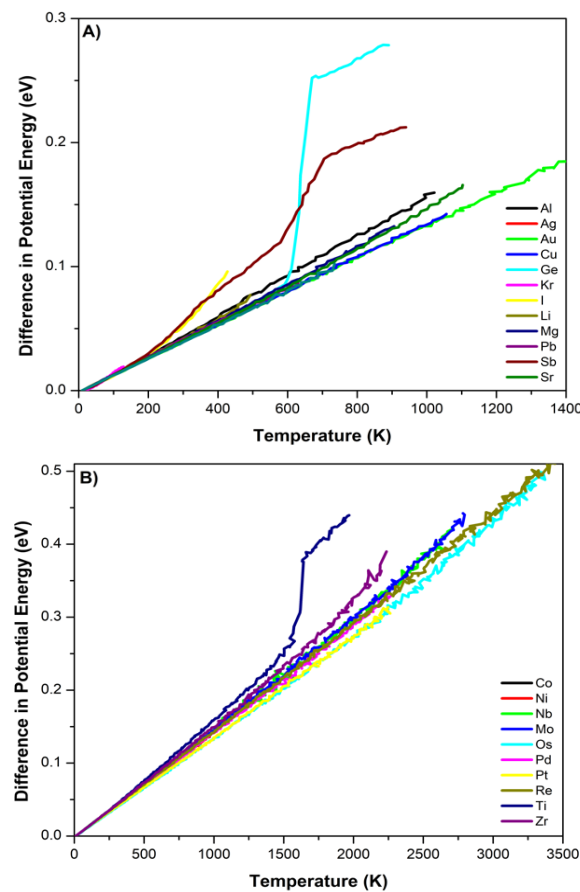


Figure 8. Potential energy vs. temperatures for all 23 DNPs generated the difference in the potential energy from 0 K for each element with A) element with melting temperatures less than 1700 K and B) element with melting temperatures over 1700 K.

4. Conclusions

We have described a general curation methodology constructing relatively small sets of DFT configurations (< 6000) for the training single-element atomistic potentials using the DeePMD-kit with a DeepPot-SE approach. Our dataset curation recipe works for a diverse sampling of elements across the periodic table, describing various benchmark materials properties with reasonable fidelity to DFT reference values. Additionally, we estimate the DNP's predictive accuracy range from the three randomized seeded versions to give a baseline range of values before the training sets are modified. Lastly, we find that these compact training sets, along with the DNP training approach, produced highly robust and transferrable potentials that can predict many properties that were not explicitly included in the training data. Ultimately, this work will allow users to augment and build upon these small datasets and/or curation methodologies for their unique scientific queries.

Lastly, we note various limitations and future extensions of and to this work that would benefit the community. Using these hand-curated systematic training datasets, we only focused on DeepPot-SE approach and did not assess other MLP models. Such a comparative investigation of MLPs, similar to Zuo et al.²⁷ or Morrow et al.⁵³ would be helpful to the community to assess the fidelity of the dataset + model combination. We hope this work, particularly the developed and shared datasets, will motivate such extensive comparative studies. Additionally, informative metrics describing the DFT training dataset parameters such as structural, energies, and forces landscapes would be beneficial for evaluating and comparing training datasets regardless of the MLP model employed. We posse that these future works would be highly informative for all atomistic potential development and benchmarking going forward.

Author Contributions

Christopher M. Andolina: conceptualization, data curation, formal analysis, investigation, methodology, resources, software, validation, visualization, writing – original draft. **Wissam A. Saidi:** conceptualization, formal analysis, funding acquisition, investigation, methodology, project administration, resources, software, supervision, writing – review & editing. Both authors discussed the results and reviewed the manuscript.

Conflicts of interest

There are no conflicts to declare.

Acknowledgments

We are grateful to the U.S. National Science Foundation (Award No. CSSI-2003808). We acknowledge R. Saidi for helping with

Figure 1. Computational support was provided in part by the University of Pittsburgh Center for Research Computing

through the resources provided on the H2P cluster, which is supported by NSF (Award No. OAC-2117681).

Notes and references

1. J. Behler and G. Csányi, *Euro. Phys. J. B*, 2021, **94**, 142.10.1140/epjb/s10051-021-00156-1
2. A. M. Miksch, T. Morawietz, J. Kästner, A. Urban and N. Artrith, *Mach. Learn.: Sci. Technol.*, 2021, **2**, 031001.10.1088/2632-2153/abfd96
3. J. Behler, *J. Chem. Phys.*, 2016, **145**, 170901.10.1063/1.4966192
4. Y. Mishin, *Acta Mater.*, 2021, **214**, 116980.10.1016/j.actamat.2021.116980
5. Z. Guo, D. Lu, Y. Yan, S. Hu, R. Liu, G. Tan, N. Sun, W. Jiang, L. Liu and Y. Chen, 2022
6. J. F. Rodrigues, Jr., L. Florea, M. C. F. de Oliveira, D. Diamond and O. N. Oliveira, Jr., *Discov. Mater.*, 2021, **1**, 12.10.1007/s43939-021-00012-0
7. J. Westermayr, S. Chaudhuri, A. Jeindl, O. T. Hofmann and R. J. Maurer, *Digit. Discov.*, 2022, **1**, 463-475.10.1039/d2dd00016d
8. M. Haghighatlari, J. Li, X. Guan, O. Zhang, A. Das, C. J. Stein, F. Heidar-Zadeh, M. Liu, M. Head-Gordon, L. Bertels, H. Hao, I. Leven and T. Head-Gordon, *Digit. Discov.*, 2022, **1**, 333-343.10.1039/d2dd00008c
9. V. Zaverkin, D. Holzmüller, I. Steinwart and J. Kästner, *Digit. Disc.*, 2022, **1**, 605-620.10.1039/d2dd00034b
10. M. J. Burn and P. L. A. Popelier, *Digit. Disc.*, 2023, DOI: 10.1039/d2dd00082b.10.1039/d2dd00082b
11. L. Ward and C. Wolverton, *Curr. Opin. Solid State Mater. Sci.*, 2017, **21**, 167-176.10.1016/j.cossms.2016.07.002
12. S. Käser, L. I. Vazquez-Salazar, M. Meuwly and K. Töpfer, *Digit. Disc.*, 2023, DOI: 10.1039/d2dd00102k.10.1039/d2dd00102k
13. D. Bayerl, C. M. Andolina, S. Dwaraknath and W. A. Saidi, *Digit. Disc.*, 2022, **1**, 61-69.10.1039/d1dd00005e
14. C. M. Andolina, J. G. Wright, N. Das and W. A. Saidi, *Phys. Rev. Mater.*, 2021, **5**, 083804.10.1103/PhysRevMaterials.5.083804
15. C. M. Andolina, M. Bon, D. Passerone and W. A. Saidi, *J. Phys. Chem. C*, 2021, **125**, 17438-17447.10.1021/acs.jpcc.1c04403
16. C. M. Andolina, P. Williamson and W. A. Saidi, *J. Chem. Phys.*, 2020, **152**, 154701.10.1063/5.0005347
17. W. Chu, W. A. Saidi and O. V. Prezhdo, *ACS Nano*, 2020, **14**, 10608-10615.10.1021/acsnano.0c04736
18. B. Wang, W. Chu, Y. Wu, D. Casanova, W. A. Saidi and O. V. Prezhdo, *Journal of Physical Chemistry Letters*, 2022, **13**, 5946-5952.10.1021/acs.jpclett.2c01452
19. P. Wisesa, C. M. Andolina and W. A. Saidi, *J. Phys. Chem. Lett.*, 2023, **14**, 468-475.10.1021/acs.jpclett.2c03445
20. K. Lee, D. Yoo, W. Jeong and S. Han, *Comput. Phys. Commun.*, 2019, **242**, 95-103.https://doi.org/10.1016/j.cpc.2019.04.014
21. G. Sivaraman, L. Gallington, A. N. Krishnamoorthy, M. Stan, G. Csányi, Á. Vázquez-Mayagoitia and C. J. Benmore, *Phys. Rev. Lett.*, 2021, **126**, 156002.10.1103/PhysRevLett.126.156002
22. A. V. Shapeev, *Multi. Model. & Sim.*, 2016, **14**, 1153-1173.10.1137/15m1054183
23. A. P. Bartók, M. C. Payne, R. Kondor and G. Csányi, *Phys. Rev. Lett.*, 2010, **104**, 136403.10.1103/PhysRevLett.104.136403
24. K. Choudhary, B. DeCost, C. Chen, A. Jain, F. Tavazza, R. Cohn, C. W. Park, A. Choudhary, A. Agrawal, S. J. L. Billinge, E. Holm, S. P. Ong and C. Wolverton, *npj Comput. Mater.*, 2022, **8**, 59.10.1038/s41524-022-00734-6

25. A. Y.-T. Wang, R. J. Murdock, S. K. Kauwe, A. O. Oliynyk, A. Gurlo, J. Brdoch, K. A. Persson and T. D. Sparks, *Chem. Mater.*, 2020, **32**, 4954-4965.10.1021/acs.chemmater.0c01907

26. J. Hill, G. Mulholland, K. Persson, R. Seshadri, C. Wolverton and B. Meredig, *MRS Bull.*, 2016, **41**, 399-409.10.1557/mrs.2016.93

27. Y. Zuo, C. Chen, X. Li, Z. Deng, Y. Chen, J. Behler, G. Csányi, A. V. Shapeev, A. P. Thompson, M. A. Wood and S. P. Ong, *J. Phys. Chem. A*, 2020, **124**, 731-745.10.1021/acs.jpca.9b08723

28. D. Zhang, H. Bi, F.-Z. Dai, W. Jiang, L. Zhang and H. Wang, *arXiv preprint arXiv:2208.08236*, 2022

29. Y. Zhang, H. Wang, W. Chen, J. Zeng, L. Zhang, H. Wang and W. E, *Comput. Phys. Commun.*, 2020, **253**, 107206.https://doi.org/10.1016/j.cpc.2020.107206

30. A. Jain, S. P. Ong, G. Hautier, W. Chen, W. D. Richards, S. Dacek, S. Cholia, D. Gunter, D. Skinner, G. Ceder and K. A. Persson, *APL Mater.*, 2013, **1**, 011002.10.1063/1.4812323

31. *Journal*, 2023

32. T. Wen, L. Zhang, H. Wang, E. Weinan and D. J. Srolovitz, *Mater. Futures*, 2022

33. A. Jain, G. Hautier, C. J. Moore, S. Ping Ong, C. C. Fischer, T. Mueller, K. A. Persson and G. Ceder, *Comput. Mater. Sci.*, 2011, **50**, 2295-2310.10.1016/j.commatsci.2011.02.023

34. P. Hirel, *Comput. Phys. Commun.*, 2015, **197**, 212-219.10.1016/j.cpc.2015.07.012

35. J. P. Perdew, K. Burke and M. Ernzerhof, *Phys. Rev. Lett.*, 1996, **77**, 3865-3868.10.1103/PhysRevLett.77.3865

36. P. E. Blochl, *Phys. Rev. B*, 1994, **50**, 17953-17979.10.1103/physrevb.50.17953

37. G. Kresse and D. Joubert, *Phys. Rev. B*, 1999, **59**, 1758

38. A. Jain, G. Hautier, S. P. Ong, C. J. Moore, C. C. Fischer, K. A. Persson and G. Ceder, *Phys. Rev. B*, 2011, **84**, 045115.10.1103/PhysRevB.84.045115

39. M. Methfessel and A. T. Paxton, *Phys. Rev. B*, 1989, **40**, 3616-3621.10.1103/physrevb.40.3616

40. H. Wang, L. Zhang, J. Han and W. E, *Comput. Phys. Commun.*, 2018, **228**, 178-184.10.1016/j.cpc.2018.03.016

41. J. H. Linfeng Zhang, Han Wang, Wissam A. Saidi, Roberto Car, Weinan E, 2018

42. M. de Jong, W. Chen, T. Angsten, A. Jain, R. Notestine, A. Gamst, M. Sluiter, C. Krishna Ande, S. van der Zwaag, J. J. Plata, C. Toher, S. Curtarolo, G. Ceder, K. A. Persson and M. Asta, *Sci. Data*, 2015, **2**, 150009.10.1038/sdata.2015.9

43. P. Hirel, *Comput. Phys. Comm.*, 2015, **197**, 212-219.10.1016/j.cpc.2015.07.01

44. K. Dang, J. Chen, B. Rodgers and S. Fensin, *Comput. Phys. Commun.*, 2023, **286**, 108667

45. A. Jain, S. P. Ong, G. Hautier, W. Chen, W. D. Richards, S. Dacek, S. Cholia, D. Gunter, D. Skinner, G. Ceder and K. A. Persson, *APL Materials*, 2013, **1**, 011002.10.1063/1.4812323

46. W. Xu and J. A. Moriarty, *Phys. Rev. B*, 1996, **54**, 6941-6951.10.1103/PhysRevB.54.6941

47. L. J. Munro and D. J. Wales, *Phys. Rev. B*, 1999, **59**, 3969-3980.10.1103/PhysRevB.59.3969

48. G. Vérité, C. Domain, C.-C. Fu, P. Gasca, A. Legris and F. Willaime, *Phys. Rev. B*, 2013, **87**, 134108.10.1103/PhysRevB.87.134108

49. J. Wu, Y. Zhang, L. Zhang and S. Liu, *Phys. Rev. B*, 2021, **103**.10.1103/PhysRevB.103.024108

50. A. V. Ruban, H. L. Skriver and J. K. Nørskov, *Phys. Rev. B*, 1999, **59**, 15990-16000.10.1103/PhysRevB.59.15990

51. H. Zhuang, A. J. Tkalych and E. A. Carter, *J. Phys. Chem. C*, 2016, **120**, 23698-23706.10.1021/acs.jpcc.6b09687

52. R. Chahal, S. Roy, M. Brehm, S. Banerjee, V. Bryantsev and S. T. Lam, *JACS Au*, 2022, **2**, 2693-2702.10.1021/jacsau.2c00526

53. J. D. Morrow, J. L. A. Gardner and V. L. Deringer, *J. Chem. Phys.*, 2023, **158**.10.1063/5.0139611